MITSUBISHI ELECTRIC RESEARCH LABORATORIES
http://www.merl.com

Station keeping and momentum management of low-thrust satellites using MPC

Weiss, Avishai; Kalabić, Uroš; Di Cairano, Stefano

TR2018-048 July 10, 2018

Abstract

This work proposes a Model Predictive Control (MPC) policy for simultaneous station keeping and momentum management of a low-thrust nadir-pointing satellite in geostationary orbit around the Earth. The satellite is equipped with six electrically powered thrusters and three axisymmetric reaction wheels, which must be coordinated to control the satellite orbital position and, concurrently, unload the wheels' stored angular momentum. The MPC policy enforces constraints that maintain the satellite in a tight latitude and longitude window and in a tight nadir-pointing attitude configuration, while minimizing the delta-v provided by the thrusters. The MPC policy exploits a prediction model of the environmental disturbance forces in order to significantly reduce the delta-v required for station keeping, and enforces constraints determined by the thruster configuration to select control forces and torques that can be generated by the propulsion system. Numerical simulations of the control policy in closed-loop with the satellite nonlinear dynamics under high-precision orbit propagation provided by Systems Tool Kit (STK) that validate the performance of the proposed design in terms of thruster usage and constraint enforcement are presented.

Aerospace Science and Technology

Aerospace Science and Technology 76 (2018) 229–241

Contents lists available at ScienceDirect

Aerospace Science and Technology

www.elsevier.com/locate/aescte

Station keeping and momentum management of low-thrust satellites using MPC

Avishai Weiss *, Uroš V. Kalabić, Stefano Di Cairano

Mitsubishi Electric Research Labs, Cambridge, MA 02139, United States

ARTICLE INFO

Article history:
Received 28 June 2017
Received in revised form 28 November 2017
Accepted 9 February 2018
Available online 14 February 2018

ABSTRACT

This work proposes a Model Predictive Control (MPC) policy for simultaneous station keeping and momentum management of a low-thrust nadir-pointing satellite in geostationary orbit around the Earth. The satellite is equipped with six electrically powered thrusters and three axisymmetric reaction wheels, which must be coordinated to control the satellite's orbital position and, concurrently, unload the wheels' stored angular momentum. The MPC policy enforces constraints that maintain the satellite in a tight latitude and longitude window and in a tight nadir-pointing attitude configuration, while minimizing the delta-v provided by the thrusters. The MPC policy exploits a prediction model of the environmental disturbance forces in order to significantly reduce the delta-v required for station keeping, and enforces constraints determined by the thruster configuration to select control forces and torques that can be generated by the propulsion system. Numerical simulations of the control policy in closed-loop with the satellite nonlinear dynamics under high-precision orbit propagation provided by Systems Tool Kit (STK) that validate the performance of the proposed design in terms of thruster usage and constraint enforcement are presented.

1. Introduction

Satellites in geostationary Earth orbit (GEO) are subject to various non-Keplerian forces and disturbance torques that affect their ability to maintain station and nadir-pointing attitude [1, Ch. 9], [2, Ch. 8]. However, for proper operation, and in order to not interfere with other spacecraft, the position and attitude of a GEO satellite must be maintained within tight pre-specified ranges. When these operating conditions are met, the satellite appears as a fixed point in the sky, collisions with other bodies cannot take place, and body-fixed satellite equipment, such as antennas and dishes, are properly oriented. Thus, to counteract the disturbance forces and torques so as to meet these operational requirements, GEO satellites are often equipped with thrusters for station-keeping (SK) maneuvers, and reaction wheels for momentum management (MM).

A GEO satellite is assigned a station-keeping window, a rectangular region above the Earth, whose sides are lines of longitude and latitude [3, Ch. 5], [4,5]. Conventionally, satellites in GEO use chemical propulsion for SK within this window. The propulsion system is manually commanded from the ground to fire roughly once every two weeks in order to compensate for secular and periodic perturbations that force the satellite outside of its station-keeping window. SK maneuvers that a GEO satellite performs are typically small but, over an ordinary satellite lifetime of twelve to fifteen years, the total Delta-v required is substantial. Thus, a significant amount of the mass of the satellite is fuel, reducing the available payload. For surveys on conventional SK, see [6,7] and references therein. In recent years, GEO satellites have begun to utilize electric propulsion, which is a more efficient alternative to chemical propulsion. Electric thrusters [8, Ch. 1], [9,10] have significantly higher specific impulse I_{sp} than conventional chemical thrusters, meaning that they generate force more efficiently with respect to propellant mass, and can therefore be used to increase spacecraft longevity, and/or increase payloads, and/or decrease the cost of orbital insertion. Since these considerations are becoming more important, electric propulsion has been slowly overcoming resistance that has heretofore hindered its use in application [11, 12]. Nonetheless, high-efficiency electric thrusters generate thrust that is on the order of one hundredth the magnitude of chemical thrusters and this poses new challenges in their use.

In addition to orbital perturbations, GEO satellites are disturbed by environmental torques that perturb the attitude of the satellite. Momentum management of GEO satellites is thus needed in order to counteract these disturbance torques. Since the attitude of the satellite must be tightly controlled, the disturbance torques

* Corresponding author.
E-mail address: weiss@merl.com (A. Weiss).

https://doi.org/10.1016/j.ast.2018.02.014
1270-9638/

Nomenclature

A	discrete-time system matrix
A_c	continuous-time system matrix
B	discrete-time input matrix
B_c	continuous-time input matrix
C_{srp}	solar radiation pressure constant ..... kN/m^2
F_x, F_y, F_z	external force coordinates ..... N
J_2	geopotential perturbation model coefficient
J_b	satellite bus moment of inertia ..... kg m^2
J_{sc}	satellite total moment of inertia ..... kg m^2
J_{w_i}	ith reaction wheel moment of inertia ..... kg m^2
R	satellite attitude matrix
S	satellite solar-facing surface area ..... m^2
$\delta\vec{r}$	satellite position vector with respect to target location ..... km
$\delta x, \delta y, \delta z$	satellite relative coordinates ..... km
$\delta\omega_1, \delta\omega_2, \delta\omega_3$	satellite relative angular velocity coordinates ..... rad/s
$\delta\psi, \delta\theta, \delta\phi$	3-2-1 satellite relative Euler angles ..... rad
η	reaction wheel acceleration command ..... rad/s^2
η_1, η_2, η_3	reaction wheel acceleration command coordinates ..... rad/s^2
$\hat{k}_E$	z-axis unit vector of the Earth-centered inertial frame
$\lambda_{1,max}$	maximum longitude error ..... rad
$\lambda_{2,max}$	maximum latitude error ..... rad
μ	gravitational parameter ..... km^3/s^2
μ_{moon}	lunar gravitational parameter ..... km^3/s^2
μ_{sun}	solar gravitational parameter ..... km^3/s^2
ν_i	ith reaction wheel angular rate ..... rad/s
ω	satellite angular velocity ..... rad/s
ψ, θ, ϕ	satellite 3-2-1 Euler angles ..... rad
ρ_E	Earth's equatorial radius ..... km
τ	satellite thruster torque ..... N m
τ_1, τ_2, τ_3	satellite thruster torque coordinates ..... N m
$\vec{F}$	external force vector ..... N
$\vec{a}_p$	perturbation acceleration vector ..... km/s^2
$\vec{r}$	satellite position vector with respect to center of Earth ..... km
$\vec{r}_0$	nominal orbital position vector ..... km
$a_{p,x}, a_{p,y}, a_{p,z}$	perturbation acceleration coordinates ..... km/s^2
c_{refl}	satellite surface reflectance
m	satellite mass ..... kg
n	mean motion ..... rad/s
u	control vector
x	state vector

must be absorbed by onboard momentum exchange devices such as reaction wheels. However, as reaction wheels cannot spin at arbitrarily high rates, there is a limit to the amount of disturbance torques that a satellite may absorb. Therefore, to prevent saturation of the wheels and subsequent loss of the desired satellite attitude, the angular momentum stored by the wheels must be periodically unloaded. Momentum unloading is often a manually controlled operation [13–15], whereby a set of thrusters, different from those used for SK and often producing much less thrust, are commanded to fire in order to lower the reaction wheels' spin rates. Thus, in order to further reduce the mass of the spacecraft propulsion system, it is desirable to utilize the same set of thrusters for both SK and momentum unloading. Electric thrusters, producing lower amounts of thrust and thereby allowing for finer control, can be used for this purpose. When the same set of thrusters is used for both station keeping and momentum management, the two usually decoupled objectives of orbital and attitude control become coupled through constraints on the propulsion system.

In this work, we consider simultaneous station keeping and momentum management (SK-MM) of satellites equipped with electric propulsion systems. Since electric propulsion produces thrust on the order of magnitude of GEO perturbation forces [12, 16], electric thrusters have to fire continuously in order to impart a response that is equivalent to that of a chemical thruster. Thus, due to the low thrust of the propulsion system and due to the fact that the same thrusters are used for both SK and MM, the conventional, impulsive, control approaches may not be appropriate.

Much of the research on low-thrust SK has thus far focused on open-loop optimal maneuver design, e.g., [17–21]. Here, we consider onboard feedback control algorithms that continuously adjust the thrusters without constant supervision of a ground control center. The satellite thus performs SK-MM operations autonomously and concurrently. Developing the capability of closed-loop control is attractive [3, Ch. 8.2], [22, Ch. 11.7]. Satellite co-location and the relatively high density of the GEO belt requires that satellites be placed in tight SK windows, and it can be expected that such SK windows will become even smaller in the next few years due to the increasing amount of satellites in the GEO belt. Smaller SK windows necessitate more frequent control, which would place an excessively large burden on ground control operators. Thus, closed-loop control allows for a greater degree of satellite autonomy, and reduces the need of constant supervision from ground control centers, which helps to increase the number of objects in the sky without increasing the fixed infrastructure of ground control centers. Additionally, onboard autonomous operation has the potential to reduce cost and risk by removing operator and communication errors. However, the onboard implementation of the control algorithm also introduces challenging limitations. Feedback control algorithms tend to operate with update rates that are faster than those of open-loop control algorithms, being focused on rejecting disturbances by using feedback from sensors. Most importantly, the computational capabilities of the on-board computing platform are significantly reduced with respect to those of ground control centers, i.e., embedded systems as opposed to mainframes and clusters. As a consequence, the onboard control algorithm needs to be lightweight compared to those executed in ground control centers, and to complete the computations within the allocated execution period. Furthermore, the computational routines of the control algorithm need to be relatively simple to allow for rapid and thorough verification, as required for the certification of autonomous systems. The salient features of the coordinated SK-MM problem include continuous control, fuel-efficiency maximization, ability to meet tight SK window and attitude error requirements, stringent constraints on available thrust, and the coordination between orbital and attitude control. Considering the above, it is clear that the SK-MM problem is an ideal candidate for model predictive control (MPC). MPC [23, Ch. 2] is a receding horizon control strategy that exploits a prediction model of the system dynamics in order to attain a trajectory that minimizes a cost function, possibly accounting for several control objectives, subject to both state and control constraints over a finite future prediction horizon. Research has been done to apply MPC in the context of low thrust propulsion for interplanetary rendezvous [24], and attitude control [25].

When nonlinear prediction models are used within MPC, the resulting optimization problem is non-convex [23, Chapter 2],

and hence convergence to the global optimum cannot be guaranteed [26, Chapter 4] unless global optimization techniques such as dynamic programming or sampling based techniques are applied. However, these methods tend to be computationally demanding as the system dimension increases due to the curse of dimensionality [27, Ch. 6]. Since our aim is to develop algorithms that can be executed onboard, in this work we develop a feedback control algorithm in the form of a linear-quadratic constrained model predictive control. The proposed algorithm autonomously coordinates the SK and MM operations, enforcing the specification constraints of proper operation, while attempting to maximize fuel-efficiency. At the same time, during execution, only quadratic programming (QP) problems need to be solved, for which several fast and low complexity algorithms have been developed in recent years for embedded system execution [28–35]. While using a linear-quadratic MPC induces some approximations in the prediction of the satellite dynamics, due to the tight SK-MM requirements around the satellite operating point, we expect the prediction to be accurate over the constraint-admissible operating range, and we rely on the inherent robustness of the feedback nature of MPC to reject the errors caused by such approximations, while still achieving correct and effective satellite operation.

The MPC prediction model developed in this work is based on the linearization of the satellite dynamics around their nominal operating condition. To compute the satellite's position and velocity relative to a target location in GEO, we use Euler angles to represent the attitude of the satellite relative to the nadir-pointing local-vertical, local-horizontal (LVLH) frame, and we use the Clohessy–Wiltshire Hill (CWH) equations for orbital position. The MPC scheme enforces constraints relating to the size of the SK window, the maximum allowed satellite attitude error, and the limits on thrust magnitude. To handle major perturbation forces, we incorporate a predicted disturbance sequence into our MPC model with the use of analytic expressions. Such disturbance models allows the MPC to increase the fuel efficiency of the solution; as an example, our simulations show that the MPC scheme is able to compute fuel efficient maneuvers by taking advantage of the coupling in the orbital plane of the CWH dynamic equations.

The proposed control method is validated through numerical simulations. In our simulations, we have utilized numerical integration of the full nonlinear governing equations and perturbation forces. The results show that MPC is able to achieve fuel-efficient SK-MM maneuvers while satisfying all the satellite operation constraints. For additional validation, we have performed simulations using the Systems Tool Kit (STK)/Astrogator®, a high-fidelity orbit propagator in order to validate both our nonlinear model and the applicability of our MPC design to real-world implementation. In such simulations we have closed the loop between the MPC policy and the STK Astrogator propagator where, during each sampling period, the MPC policy computes the control commands and sends them to the STK propagator, which then uses them to update the orbital position and returns the new satellite conditions to the controller for use during the next sampling period.

Preliminary versions of some results in this paper have appeared in various conference publications [36–38]. In this work, we expand upon those by providing additional details on the model and on the control design, adding discussions on the computational feasibility of our algorithm for on-board implementation, providing more simulation results, and including a validation of our simulations under high-precision orbit propagation provided by STK. Overall, this paper contains more details, case studies, interpretations, and discussion.

The paper is organized as follows. In Section 2 we present the kinematics and dynamics of a nadir-pointing satellite in GEO and review the main orbital perturbations it experiences. In Section 3 we present the formulation of the optimization problem

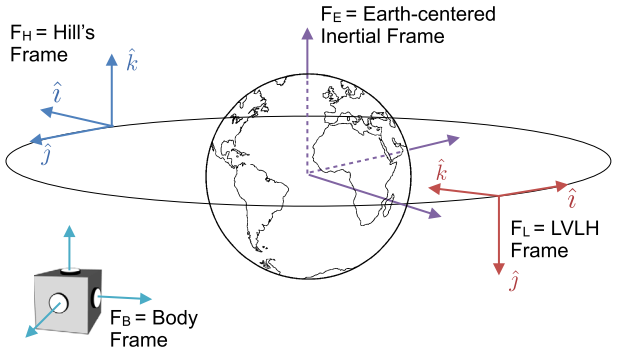

Fig. 1. Inertial and non-inertial frames used for describing the satellite dynamics.

constraints and develop the MPC policy. Section 4 highlights the proposed strategy on numerical examples and presents the validation results from STK. Finally, we provide concluding remarks and thoughts on future research directions in Section 5.

2. Kinematic and dynamic models

In this section, we review the nonlinear and linearized orbital and attitude dynamics of geostationary satellites and present analytical expressions for the main perturbations that affect satellites in GEO.

2.1. Notation

The vector $\vec{r}_{q/p}$ denotes the position of point q relative to point p, the vector $\vec{v}_{q/p/X}$ denotes the velocity of point q relative to point p with respect to frame F_X, and the vector $\vec{\omega}_{Y/X}$ denotes the angular velocity of frame F_Y relative to frame F_X. Note that $\vec{(\cdot)}$ denotes a coordinate-free (unresolved) vector. All frames are orthogonal and right-handed.

2.2. Satellite orbital dynamics

The relative position vector of a satellite with respect to a target location on an orbit is expressed as

$$\delta\vec{r} = \delta x\hat{\imath} + \delta y\hat{\jmath} + \delta z\hat{k},$$

where δx, δy and δz are the components of the position vector of the satellite relative to the target location and $\hat{\imath}$, $\hat{\jmath}$, $\hat{k}$ are the unit vectors of Hill's frame F_H. In Hill's frame F_H, the y-axis is in the direction of satellite velocity, the x-axis is in the radial direction pointing away from the Earth, and z-axis is in the direction of angular momentum. Hill's frame can be visualized in Fig. 1, along with the inertial Earth-centered frame F_E, the LVLH frame F_L, and the satellite body-fixed frame F_B.

The position vector of the satellite with respect to the center of the Earth is given by $\vec{r} = \vec{r}_0 + \delta\vec{r}$, where $\vec{r}_0$ is the nominal orbital position vector. The nonlinear equation of motion for the satellite relative to inertial frame F_E is given by

$$\ddot{\vec{r}} = -\mu\frac{\vec{r}}{r^3} + \frac{1}{m}\vec{F} + \vec{a}_p, \tag{1}$$

where $\vec{F}$ is the vector of external forces applied to the satellite by the thrusters, $\vec{a}_p$ is the vector of perturbation accelerations, $r = |\vec{r}|$ is the distance of the satellite from Earth's center of gravity, m is the mass of the satellite, and μ is Earth's gravitational constant.

For small maneuvers around a nominal circular orbit, for which $\delta r \ll r$, the linearized CWH equations [39], [40, pg. 300] approximate the relative motion of the satellite as

$$\begin{aligned} \delta\ddot{x} - 3n^2\delta x - 2n\delta\dot{y} &= \frac{F_x}{m} + a_{\mathrm{p},x}, \\ \delta\ddot{y} + 2n\delta\dot{x} &= \frac{F_y}{m} + a_{\mathrm{p},y}, \\ \delta\ddot{z} + n^2\delta z &= \frac{F_z}{m} + a_{\mathrm{p},z}, \end{aligned} \tag{2}$$

where F_x, F_y, F_z are components of the thrust force vector, $a_{\mathrm{p},x}, a_{\mathrm{p},y}, a_{\mathrm{p},z}$ are components of the perturbation acceleration vector, and $n = \sqrt{\frac{\mu}{R_0^3}}$ denotes the mean motion of the nominal orbit. The linearized dynamics account for differences in gravity between the satellite and nominal orbital location. The satellite dynamics in the orbital plane (x–y) and in the out-of-orbital axis (z) are decoupled. The in-plane dynamics are Lyapunov unstable, with 2 eigenvalues at the origin and 2 eigenvalues on the imaginary axis at $\pm n$, while the out-of-plane dynamics are marginally Lyapunov stable, with 2 eigenvalues on the imaginary axis at $\pm n$.

2.3. Satellite attitude kinematics

The satellite's attitude is determined by Poisson's equation,

$$\dot{R}(t) = R(t)\omega^{\times}(t), \tag{3}$$

where $\omega(t) \in \mathbb{R}^3$ is the angular velocity of the satellite bus frame $\mathrm{F_B}$ with respect to the inertial frame $\mathrm{F_E}$ resolved in the satellite frame, $\omega^{\times}(t)$ is the cross-product matrix of $\omega(t)$, and $R(t) = \mathcal{O}_{\mathrm{E/B}}(t) \in \mathbb{R}^{3\times 3}$ is the rotation matrix, resolved in the satellite frame, that transforms the inertial frame into the satellite frame. Therefore, $R(t)$ is the proper orthogonal matrix (that is, the rotation matrix) that transforms the components of a vector resolved in the satellite frame into the components of the same vector resolved in the inertial frame.

The attitude R of a nadir-pointing satellite on a circular geostationary orbit must follow an attitude trajectory given by a time-varying continuously differentiable rotation matrix $R_{\mathrm{d}}(t) = \mathcal{O}_{\mathrm{E/L}}(t)$ so that the bus-fixed frame $\mathrm{F_B}$ aligns with the LVLH frame $\mathrm{F_L}$. For $t \geq 0$, $R_{\mathrm{d}}(t)$ is given by

$$\begin{aligned} \dot{R}_{\mathrm{d}}(t) &= R_{\mathrm{d}}(t)\omega_{\mathrm{d}}^{\times}(t), \\ R_{\mathrm{d}}(0) &= R_{\mathrm{d0}}, \end{aligned} \tag{4}$$

where $\omega_{\mathrm{d}}(t)$ is the desired angular velocity and, for a nadir-pointing satellite in GEO, is given by a constant spin about the axis perpendicular to the orbital plane with a period of one sidereal day.

The error between $R(t)$ and $R_{\mathrm{d}}(t)$ is given in terms of the attitude-error rotation matrix

$$\tilde{R} \triangleq R^{\mathrm{T}}R_{\mathrm{d}} = \mathcal{O}_{\mathrm{E/B}}^{\mathrm{T}}\mathcal{O}_{\mathrm{E/L}} = \mathcal{O}_{\mathrm{B/L}}. \tag{5}$$

Because we are considering small motions about an equilibrium, we parameterize the attitude-error rotation matrix $\tilde{R}$ using a set of 3-2-1 Euler angles (ψ, θ, ϕ), where $\tilde{R} = C_1(\phi)C_2(\theta)C_3(\psi)$ and C_1, C_2, and C_3 are elementary rotations about the x, y, and z-axes by the angles ψ, θ, and ϕ, respectively. The angular velocity $\omega = \vec{\omega}_{\mathrm{B/E}}\big|_{\mathrm{B}}$ is thus given by

$$\begin{aligned} \vec{\omega}_{\mathrm{B/E}}\big|_{\mathrm{B}} &= \left(\vec{\omega}_{\mathrm{B/L}} + \vec{\omega}_{\mathrm{L/E}}\right)\big|_{\mathrm{B}} = \left(\vec{\omega}_{\mathrm{B/L}} - n\hat{e}_y\right)\big|_{\mathrm{B}}, \\ &= \begin{bmatrix} \dot{\phi} \\ 0 \\ 0 \end{bmatrix} + C_1(\phi)\begin{bmatrix} 0 \\ \dot{\theta} \\ 0 \end{bmatrix} + C_1(\phi)C_2(\theta)\begin{bmatrix} 0 \\ 0 \\ \dot{\psi} \end{bmatrix} \\ &\quad - n\mathcal{O}_{\mathrm{B/L}}\begin{bmatrix} 0 \\ 1 \\ 0 \end{bmatrix}. \end{aligned} \tag{6}$$

Let $\omega_{\mathrm{d}} = \begin{bmatrix} 0 & -n & 0 \end{bmatrix}^{\mathrm{T}}$, the linearization of (6) about ω_{d} yields

$$\begin{aligned} \delta\dot{\phi} &= \delta\omega_1 + n\delta\psi, \\ \delta\dot{\theta} &= \delta\omega_2, \\ \delta\dot{\psi} &= \delta\omega_3 - n\delta\phi. \end{aligned} \tag{7}$$

2.4. Attitude dynamics for a satellite with reaction wheels

Consider a satellite actuated by three axisymmetric wheels $\mathrm{w}_1, \mathrm{w}_2, \mathrm{w}_3$, each with moment of inertia $J_{\mathrm{w}_i} = \mathrm{diag}(\alpha_i, \beta_i, \beta_i)$, attached to a rigid bus b with moment of inertia $J_{\mathrm{b}} = \mathrm{diag}(J_{\mathrm{b}_1}, J_{\mathrm{b}_2}, J_{\mathrm{b}_3})$ in an orthogonal configuration aligned with the principal axes of the bus. The wheels are mass-balanced relative to the center of mass of the bus so that the center of mass of the satellite coincides with the center of mass of the bus. Each wheel w_i is mounted so that it rotates about one of its own principal axes passing through its own center of mass with angular rate ν_i. Assume a bus-fixed frame $\mathrm{F_B}$, three wheel-fixed frames $\mathrm{F_{W_1}}, \mathrm{F_{W_2}}, \mathrm{F_{W_3}}$, whose x-axes are aligned with the rotation axes of $\mathrm{w}_1, \mathrm{w}_2, \mathrm{w}_3$, respectively, and an inertial frame $\mathrm{F_E}$. Then, the attitude dynamics of the satellite are given by [41]

$$J_{\mathrm{sc}}\dot{\omega} = (J_{\mathrm{sc}}\omega + J_\alpha\nu) \times \omega - J_\alpha\eta + \tau, \tag{8a}$$

$$\dot{\nu} = \eta, \tag{8b}$$

where $\nu \triangleq [\nu_1 \quad \nu_2 \quad \nu_3]^{\mathrm{T}}$, the vector τ represents the torque applied to the satellite from the thrusters, $J_\alpha \triangleq \mathrm{diag}(\alpha_1, \alpha_2, \alpha_3)$ is the moment of inertia of the reaction wheel array, and $J_{\mathrm{sc}} = \tilde{J}_{\mathrm{b}} + J_\alpha$ is the moment of inertia of the satellite bus and reaction wheel array, where the moments of inertia $\beta_1, \beta_2, \beta_3$ of the wheels are lumped into the bus inertia $\tilde{J}_{\mathrm{b}} = \mathrm{diag}(\tilde{J}_{\mathrm{b}_1}, \tilde{J}_{\mathrm{b}_2}, \tilde{J}_{\mathrm{b}_3})$, where $\tilde{J}_{\mathrm{b}_1} \triangleq J_{\mathrm{b}_1} + \beta_2 + \beta_3$, $\tilde{J}_{\mathrm{b}_2} \triangleq J_{\mathrm{b}_2} + \beta_1 + \beta_3$, and $\tilde{J}_{\mathrm{b}_3} \triangleq J_{\mathrm{b}_3} + \beta_1 + \beta_2$. For each wheel w_i, the wheel angular accelerations are given by η_i, where $\eta \triangleq [\eta_1 \quad \eta_2 \quad \eta_3]^{\mathrm{T}}$. Note that, in practice, a servo loop is closed around each reaction wheel in order to produce the desired wheel angular accelerations.

The linearization of (8) about an equilibrium y-axis (principal axis) spin ω_{d} with an angular rate corresponding to the mean motion n of the orbit yields

$$J_{\mathrm{sc}_1}\dot{\delta\omega}_1 = -\left(J_{\mathrm{sc}_2} - J_{\mathrm{sc}_3}\right)n\,\delta\omega_3 + n\alpha_3\delta\nu_3 - \alpha_1\eta_1 + \tau_1, \tag{9a}$$

$$J_{\mathrm{sc}_2}\dot{\delta\omega}_2 = -\alpha_2\eta_2 + \tau_2, \tag{9b}$$

$$J_{\mathrm{sc}_3}\dot{\delta\omega}_3 = -\left(J_{\mathrm{sc}_1} - J_{\mathrm{sc}_2}\right)n\,\delta\omega_1 - n\alpha_1\delta\nu_1 - \alpha_3\eta_3 + \tau_3, \tag{9c}$$

$$\delta\dot{\nu}_1 = \eta_1, \tag{9d}$$

$$\delta\dot{\nu}_2 = \eta_2, \tag{9e}$$

$$\delta\dot{\nu}_3 = \eta_3. \tag{9f}$$

2.5. Perturbations

Keplerian orbits, i.e., conic-section solutions to the two-body problem in a uniform inverse-square force field, do not exist

in practice. Without orbital correction maneuvers, satellites drift from their assigned orbital positions due to various perturbational forces. For satellites in GEO, the main perturbations are solar and lunar gravitational attraction, which induce a drift in orbital inclination, solar radiation pressure, which affects orbit eccentricity, and the anisotropic geopotential, that is, Earth's non-spherical gravitational field, which induces in-orbital-plane longitudinal drift [21], [42, Ch. 7]. Analytic expressions for these perturbation forces per unit mass, i.e., the disturbance accelerations, are given, respectively, by

$$\vec{a}_{\text{sun}} = \mu_{\text{sun}} \left(\frac{\vec{r}_{\text{sun/sc}}}{r^3_{\text{sun/sc}}} - \frac{\vec{r}_{\text{sun/earth}}}{r^3_{\text{sun/earth}}} \right), \tag{10a}$$

$$\vec{a}_{\text{moon}} = \mu_{\text{moon}} \left(\frac{\vec{r}_{\text{moon/sc}}}{r^3_{\text{moon/sc}}} - \frac{\vec{r}_{\text{moon/earth}}}{r^3_{\text{moon/earth}}} \right), \tag{10b}$$

$$\vec{a}_{\text{srp}} = C_{\text{srp}} \frac{S(1+c_{\text{refl}})}{2m} \frac{\vec{r}_{\text{sc/sun}}}{r_{\text{sc/sun}}}, \tag{10c}$$

$$\vec{a}_{J_2} = \frac{3\mu J_2 \rho_{\text{E}}^2}{2r^5} \left(\left(5\frac{(\vec{r}\cdot\hat{k}_{\text{E}})}{r^2} - 1 \right) \vec{r} - 2(\vec{r}\cdot\hat{k}_{\text{E}})\hat{k}_{\text{E}} \right), \tag{10d}$$

where μ_{sun} and μ_{moon} are the gravitational constants of the sun and moon, C_{srp} is the solar radiation pressure constant, S is the solar-facing surface area, c_{refl} is the surface reflectance, ρ_{E} is Earth's equatorial radius, $\hat{k}_{\text{E}}$ is the z-axis unit vector of the Earth-centered inertial frame F_{E}, and J_2 is the dominant coefficient in the considered geopotential perturbation model, where additional higher order terms are ignored.

The sum of the individual disturbance accelerations (10a)–(10d)

$$\vec{a}_{\text{p}} = \vec{a}_{\text{sun}} + \vec{a}_{\text{moon}} + \vec{a}_{\text{srp}} + \vec{a}_{J_2}, \tag{11}$$

yields the total disturbance acceleration considered in (1). Fig. 2a shows an annual time history of the disturbance force components for a 4000kg satellite in GEO. Fig. 2b shows the uncompensated motion of the satellite subject to the aforementioned perturbations after one month.

Satellites are also subject to environmental torques such as those due to gravity gradients, solar radiation pressure, atmospheric drag, or the ambient magnetic field. For geostationary satellites, solar radiation pressure is the dominant effect. In this work, we do not model these torques directly, but rather, we assume that they are easily absorbed by onboard reaction wheels via a nominal attitude control law. The resultant stored momentum is then treated as an initial condition.

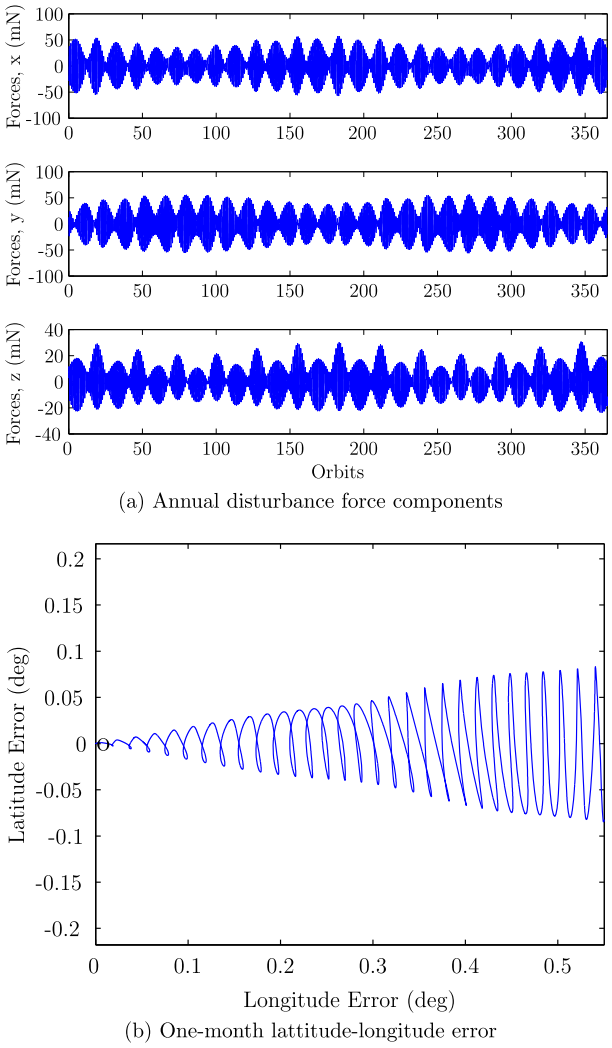

(a) Annual disturbance force components

(b) One-month lattitude-longitude error

Fig. 2. (a) Disturbance force components in Hill's Frame F_{H} and (b) Uncompensated motion for a 4000 kg satellite in geostationary orbit over one month.

3. Controller design

The control objectives considered in this work for the simultaneous station-keeping and momentum management of a geostationary satellite are:

1. Maintain the satellite in a station-keeping window
2. Maintain the satellite in a nadir-pointing configuration at all times, including during momentum unloading
3. Unload the stored angular momentum from the reaction wheels, i.e., bring wheel speeds to zero
4. Limit the requested thruster magnitudes
5. Minimize fuel consumption

In order to handle the multitude of objectives, we design an MPC policy. MPC generates control actions by solving a receding-horizon finite-time optimal control problem formulated from a system prediction model, a user-defined cost function, and state and control constraints that, for discrete-time prediction models, are enforced pointwise-in-time [23,43,44], i.e., at the sampling instants. By using linearized equations of motion, linear equality and inequality constraints, and quadratic costs on the states and control actions, the MPC policy may be formulated as a QP, which, given the limited computational resources onboard most satellites, can be solved quickly and efficiently [31]. In an MPC context, Objectives 1, 2, and 4 can be naturally represented as constraints that can be incorporated into the MPC policy since they involve variables that have to be maintained within bounds without a specific target value, and Objectives 3 and 5 can be handled by appropriate selection of the MPC cost function, since they involve variables for which convergence to a specific target is desired. Although not treated in the current design, other objectives related to reaction wheels may be desired. For example, it is straightforward to instead include limits on the angular momentum to ensure that the reaction wheel speeds remains in the desired range, but not necessarily desired to be zero. Alternatively, minimizing reaction wheel power consumption may be the desired objective, in which case a different MPC cost function may be formulated.

3.1. State-space model

We form a state-space model of the combined orbital dynamics (2), attitude kinematics (7), and attitude dynamics (9), to be used as a prediction model in the MPC policy. The model is given by

$$\dot{x}(t) = A_c x(t) + B_c u(t), \tag{12}$$

where

$$x = [\delta x \quad \delta y \quad \delta z \quad \delta \dot{x} \quad \delta \dot{y} \quad \delta \dot{z} \quad \delta\phi \quad \delta\theta \quad \delta\psi \quad \delta\omega_1 \quad \delta\omega_2 \quad \delta\omega_3 \quad \delta\nu_1 \quad \delta\nu_2 \quad \delta\nu_3]^{\mathrm{T}}, \tag{13}$$

$$u = [F_x \quad F_y \quad F_z \quad \eta_1 \quad \eta_2 \quad \eta_3 \quad \tau_1 \quad \tau_2 \quad \tau_3]^{\mathrm{T}}. \tag{14}$$

Assuming a sampling period of ΔT sec, we discretize (12), yielding

$$x_{k+1} = Ax_k + Bu_k, \tag{15}$$

where x_k is the state at time step $k \in \mathbb{Z}^+$, u_k is the control vector at the time step $k \in \mathbb{Z}^+$, and $A = \exp(A_c \Delta T)$ and $B = \int_0^{\Delta T} \exp(A_c(\Delta T - \tau))\mathrm{d}\tau B_c$ are the discretized matrices obtained based on the continuous-time system realization (A_c, B_c) in (12).

We augment (15) with a prediction model of the disturbance accelerations, obtaining

$$x_{k+1} = Ax_k + Bu_k + B_d \mathcal{O}_{H/E} a_{p,k}, \tag{16}$$

where $B_d = \int_0^{\Delta T} \exp(A_c(\Delta T - \tau))\mathrm{d}\tau I$, $a_{p,k}$ is the total disturbance acceleration predicted at time step k based on propagation of the desired nominal orbit, and $\mathcal{O}_{H/E}$ is the rotation matrix that transforms the components of $a_{p,k}$ from the inertial frame into the components of the same acceleration in Hill's frame. The addition of the disturbance prediction in (16) enables the MPC policy to exploit natural relative motion dynamics, rather than propulsion, against the disturbance acceleration.

Remark 1. We use the nominal orbit for disturbance-acceleration prediction in (16) due to the nonlinearity of the analytical expressions in (10). Since the nominal orbit is known in advance based on the propagation of (1), $a_{p,k}$ can be predicted. Since the satellite position is to be constrained in a tight station-keeping window according to Objective 1, the difference in the disturbance accelerations at the nominal orbital position and at the true satellite position is expected to be negligible. Validation with the nonlinear model presented later confirms this.

Remark 2. Note that additional corrective terms may be included in (16). For instance, satellite mass, center of mass, and thruster alignments may change over time, and the prediction model could incorporate online estimates of these model parameters. However, in this work, the rate of change of these quantities is slow with respect to the satellite dynamics. Hence, the model can be updated periodically as needed, while keeping the prediction model over the MPC horizon time invariant.

3.2. Constraints

Satellite position constraints may be imposed on δy and δz, corresponding to a station-keeping box using the relations

$$|\delta y| \leq r_0 \tan(\lambda_{1,\max}), \tag{17a}$$

$$|\delta z| \leq r_0 \tan(\lambda_{2,\max}), \tag{17b}$$

where $\lambda_{1,\max}$ is the maximum tolerable longitude error, and $\lambda_{2,\max}$ is the maximum tolerable latitude error.

We consider a satellite equipped with six dual-axis thrusters. Define

$$T \triangleq [T_1 \quad T_2 \quad T_3 \quad T_4 \quad T_5 \quad T_6],$$

where T_i is the force exerted by each dual-axis thruster. We set constraints on the individual thruster magnitudes, i.e.,

$$\|T\|_\infty \leq T_{\max}, \tag{18}$$

and relate them to constraints on the control input forces F and torques τ via the force-torque map

$$\begin{bmatrix} \mathcal{O}_{L/H} & 0 \\ 0 & I \end{bmatrix} \begin{bmatrix} F \\ \tau \end{bmatrix} = \begin{bmatrix} \Gamma & \Gamma \\ L & -L \end{bmatrix} T, \tag{19}$$

where Γ and L are appropriate full rank matrices related to the geometry of the thruster locations in the spacecraft frame. Combining (18) and (19) yields

$$\left\| \begin{bmatrix} \Gamma & \Gamma \\ L & -L \end{bmatrix}^{-1} \begin{bmatrix} \mathcal{O}_{L/H} & 0 \\ 0 & I \end{bmatrix} \begin{bmatrix} F \\ \tau \end{bmatrix} \right\|_\infty \leq T_{\max}, \tag{20}$$

which is enforced on the control input vector u and accomplishes Objective 4. Note that since Γ and L are full rank, the matrix in (20) is invertible. Here, invertibility implies that the thrusters are mounted in a manner that allows for linearly independent forces and torques to be applied to the satellite. Constraint (20) effectively couples (2) with (7) and (9), i.e., the propulsion system has to generate both forces for orbital control and torques for attitude control.

In (19) we assume $\tilde{R} = \mathcal{O}_{B/L} \approx I$, i.e., that the attitude error is small and that the satellite is in the nominal nadir-pointing configuration. Under this approximation the constraints are linear. We further note that validity of this approximation is enforced by the following attitude error constraints.

In order to maintain a nadir-pointing configuration as usually required for operational purposes by geostationary satellites, and to ensure that the linearization (7), (9) correctly approximates (3), (8), we constrain the Euler angles $(\delta\phi, \delta\theta, \delta\psi)$ to be within a small tolerance as required by Objective 2,

$$\begin{aligned} |\delta\phi| &\leq \delta\phi_{\max}, \\ |\delta\theta| &\leq \delta\theta_{\max}, \\ |\delta\psi| &\leq \delta\psi_{\max}. \end{aligned} \tag{21}$$

3.3. MPC policy

We consider the MPC policy that at any $k \in \mathbb{Z}^+$ solves the finite-horizon optimal control problem

$$\begin{aligned} \min_{U_k} \quad & x_{N|k}^{\mathrm{T}} P x_{N|k} + \sum_{h=0}^{N-1} x_{h|k}^{\mathrm{T}} Q x_{h|k} + u_{h|k}^{\mathrm{T}} R u_{h|k}, \\ \text{s.t.} \quad & x_{h+1|k} = Ax_{h|k} + Bu_{h|k} + B_d \mathcal{O}_{H/E} a_{p,h|k}, \\ & x_{0|k} = x_k, \\ & a_{p,h|k} = a_{p,k+h}, \\ & T_{\min} \leq Du_{h|k} \leq T_{\max}, \\ & \delta y_{\min} \leq \delta y_{h|k} \leq \delta y_{\max}, \\ & \delta z_{\min} \leq \delta z_{h|k} \leq \delta z_{\max}, \\ & \delta\phi_{\min} \leq \delta\phi_{h|k} \leq \delta\phi_{\max}, \\ & \delta\theta_{\min} \leq \delta\theta_{h|k} \leq \delta\theta_{\max}, \\ & \delta\psi_{\min} \leq \delta\psi_{h|k} \leq \delta\psi_{\max}, \end{aligned} \tag{22}$$

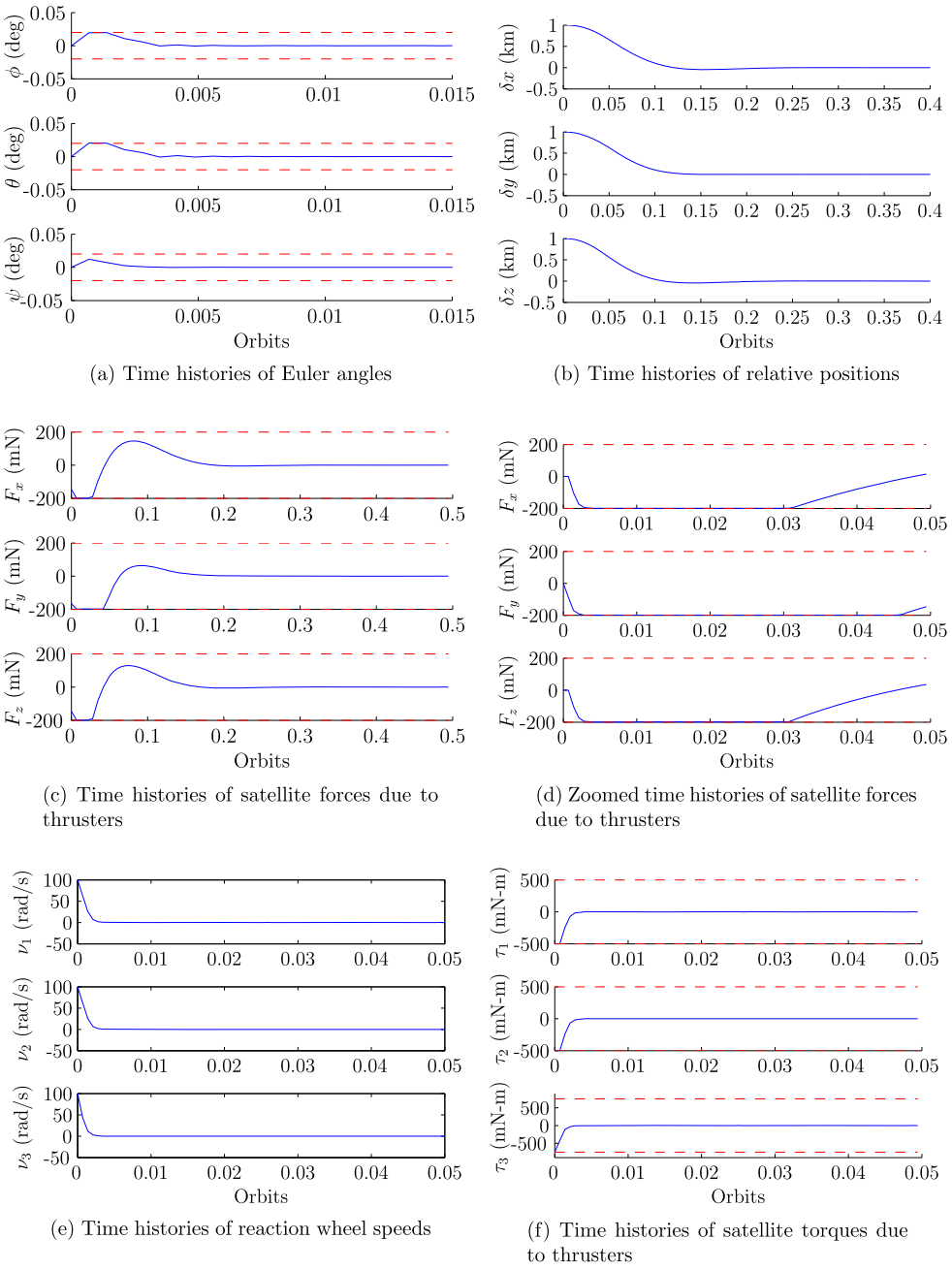

(a) Time histories of Euler angles

(b) Time histories of relative positions

(c) Time histories of satellite forces due to thrusters

(d) Zoomed time histories of satellite forces due to thrusters

(e) Time histories of reaction wheel speeds

(f) Time histories of satellite torques due to thrusters

Fig. 3. Simulation of aggressive station keeping and momentum unloading maneuver.

where the notation $z_{h|k}$ denotes the prediction of z for h steps ahead of k, N is the control and prediction horizon, Q, R are specified state and control weight matrices, D is the matrix that enforces the concurrently available forces and torques as in (20), P is the terminal state weighting matrix determined from the solution of the Discrete Algebraic Riccati Equation (DARE) for the unconstrained infinite horizon problem, and $U_k = [u_{0|k}, \ldots, u_{N-1|k}]^{\mathrm{T}}$. The policy applies $u_k = u^*_{0|k}$ to the satellite, where $[u^*_{0|k}, \ldots, u^*_{N-1|k}]^{\mathrm{T}}$ is the optimal solution of (22). The procedure is repeated at time $k+1$, with x_{k+1} as the new initial condition.

The horizon N is selected so that the MPC policy can predict and exploit the periodicity present in the dynamics and perturbations. We verify that due to strong periodicity in the dynamics over the orbit time-scale, a horizon of more than half an orbit generates Δv savings. The state and control weight matrices Q and R are selected to aggressively minimize fuel consumption and unload the reaction wheels' stored angular momentum, which accomplishes Objectives 3 and 5.

Consistent with some of the conventional MPC design approaches [45], we employ a terminal penalty matrix P based on the solution to the DARE to guarantee local asymptotic stability of the target equilibrium. Near the origin, when constraints are inactive and in the absence of disturbances, the solution of (22) is equivalent to that of the LQR controller designed based on the same dynamics and cost function. Thus, the maximum constraint admissible set O^{∞} [44] for the LQR controller under state and control constraints is a guaranteed domain of attraction for the origin, which is asymptotically stable for the system in closed loop with the MPC controller [23]. Furthermore, in the presence of disturbances, using the terminal penalty matrix P renders the system input-to-state stable [46]. In order to ensure recursive feasibility in the presence of model approximations, modeling errors, unpre-

dictable disturbances, we relax the state constraints in (22) into soft constraints by using a slack variable [47]. In general this may require slightly tightening the bounds of the state constraints to ensure that the actual specifications are met. However, as shown later in the simulation section, in all our simulations all the state constraints are always satisfied.

3.4. Numerical computation of the control command

The finite horizon optimal control problem (22) is reformulated as the parametric Quadratic Programming (pQP) problem

$$U_k^* = \arg\min_{U_k} \ \frac{1}{2}U_k' Q_\mathrm{p} U_k + \vartheta_k' C_\mathrm{p}' U_k + \frac{1}{2}\vartheta_k' \Omega_\mathrm{p} \vartheta_k, \tag{23a}$$

$$\text{s.t. } G_\mathrm{p} U_k \le S_\mathrm{p}\vartheta_k + W_\mathrm{p}, \tag{23b}$$

where the matrices Q_p, C_p, G_p, S_p, and the vector W_p are obtained, for instance, as described in [45] and the vector ϑ contains the problem parameters, i.e., the initial state and the predicted accelerations along the horizon, $\vartheta = [x'\ a_{\mathrm{p},0}' \dots a_{\mathrm{p},N-1}']'$. Since (23) is constructed from (22) at control design time and not during controller execution, the matrices in (23) are computed offline and do not impact real-time computations. During controller execution, the only operations performed in real time are substitution of $\vartheta_k = [x(k)'\ a_{\mathrm{p},k} \dots a_{\mathrm{p},k+N-1}']'$ into the pQP (23) to obtain the QP instance

$$U_k^* = \arg\min_{U_k} \ \frac{1}{2}U_k' Q_\mathrm{p} U_k + F_\mathrm{p}' U_k + M_\mathrm{p}, \tag{24a}$$

$$\text{s.t. } G_\mathrm{p} U_k \le K_\mathrm{p}, \tag{24b}$$

where $F_\mathrm{p} = C_\mathrm{p}\vartheta_k$, $K_\mathrm{p} = S_\mathrm{p}\vartheta_k + W_\mathrm{p}$, $M_\mathrm{p} = \frac{1}{2}\vartheta_k'\Omega_\mathrm{p}\vartheta_k$, computation of the solution U_k^* of (24), and generation of the control command from U_k^* as $u(k) = u_{0|k}^*$.

While the solution of the QP (24) requires nontrivial computation, several very effective algorithms exist. Interior point and active set algorithms tend to have fast convergence properties [26, Ch. 11], [48, Ch. 10]. Such algorithms reach the optimum in few iterations, but each iteration may be fairly complicated, as it requires the solution of a linear system obtained from the KKT optimality conditions. As a consequence, the code may be complicated and long, and often requires the usage of several auxiliary libraries for linear algebra. All these elements may make the on-board implementation and verification process challenging, due to limited capability of the satellite computing platform, and due to the extensive verification procedures of the hardware-software architecture for autonomous systems.

In recent years, several first order methods [49, Ch. 2] that perform computationally simple iterations have been developed for embedded control applications. Although many iterations are required to reach the optimum, the code is much simpler than the code for interior point and active set methods, e.g., few lines versus several hundreds lines of code. This simplicity enables faster implementation and verification, and suitability of the method in resource constrained hardware, which may be particularly beneficial for on-board spacecraft applications. For comparison of different algorithms tailored to MPC, including first order, interior point, and active set methods, see [50].

Recently developed first order algorithms include the fast gradient methods in [28,29], the Lagrangian method in [30], the multiplicative update in [31], and the alternating direction method of multipliers (ADMM) methods in [32–35]. As an example, the multiplicative update method in [31] solves (24) by iterating

$$[\xi_{(\ell+1)}]_i = \frac{[(Q_\mathrm{d}^- + \phi)\xi_{(\ell)} + F_\mathrm{d}^-]_i}{[(Q_\mathrm{d}^+ + \phi)\xi_{(\ell)} + F_\mathrm{d}^+]_i}[\xi_{(\ell)}]_i, \tag{25}$$

Table 1
Thruster placements.

Thruster	Position (m) in $\mathrm{F_B}$	Direction
T_1	(7.5, 0, 0)	$\hat{\jmath}_\mathrm{B}$
T_2	(0, 5, 0)	$\hat{k}_\mathrm{B}$
T_3	(0, 0, 5)	$\hat{\imath}_\mathrm{B}$
T_4	(−7.5, 0, 0)	$\hat{\jmath}_\mathrm{B}$
T_5	(0, −5, 0)	$\hat{k}_\mathrm{B}$
T_6	(0, 0, −5)	$\hat{\imath}_\mathrm{B}$

until the fixed point $\xi_{(\ell+1)} = \xi_{(\ell)}$, and then computing

$$U_k^* = \Psi_{\mathrm{d2p}}(\vartheta_k, \xi^*) = \Gamma_\mathrm{d}\vartheta_k + \Xi_\mathrm{d}\xi^*, \tag{26}$$

where in (25), (26) $F_\mathrm{d} = S_\mathrm{d}\vartheta_k + W_\mathrm{d}$, $Q_\mathrm{d} = G_\mathrm{p}Q_\mathrm{p}^{-1}G_\mathrm{p}'$, $S_\mathrm{d} = (G_\mathrm{p}Q_\mathrm{p}^{-1}C_\mathrm{p} + S_\mathrm{p})$, $\Xi_\mathrm{d} = -Q_\mathrm{p}^{-1}G_\mathrm{p}'$, $\Gamma_\mathrm{d} = -Q_\mathrm{p}^{-1}C_\mathrm{p}$, and A^+, A^- indicate the positive and negative part of the matrix A, respectively. Indeed, the code for (25), (26) can be written in less than 20 lines in standard programming languages and without any dependencies on additional libraries. Problems of the size of those generated by (22) can be solved within a few seconds even in low capability embedded computing architectures. For (22), we have verified that the solution by the algorithm based on (25) requires less than 10s on a standard 2.3 GHz Intel Core i7 laptop using only one core, and without any platform-specific compiled code optimization. The result hints at feasibility for on-board spacecraft operation, despite limited computing hardware due to, e.g., radiation hardening and constrained power limits, given that the control update period is at least several minutes.

4. Simulations

We consider a $7.5 \times 5 \times 5$ m satellite of mass $m = 4000$ kg and inertia $J_\mathrm{sc} = \mathrm{diag}(1.7e4, 2.7e4, 2.7e4)$ kg m^2 in geostationary orbit, i.e., $r_0 = 42164$ km, around the Earth. The satellite is constrained to a station-keeping window of ± 0.01 degrees longitude and latitude, while the maximum error allowed in the Euler angles is ± 0.02 degrees. The satellite is propelled by six thrusters placed according to Table 1, with $T_\mathrm{max} = 0.1$ N. From the table, we see that firing thrusters 1 and 4 with equal force in the positive direction creates a force in the direction of the y-axis and firing them with equal force in opposite directions creates a torque about the z-axis. For this simulation,

$$L = \begin{bmatrix} 0 & 2.5 & 0 \\ 0 & 0 & 2.5 \\ 3.75 & 0 & 0 \end{bmatrix}, \qquad \Gamma = \begin{bmatrix} 0 & 0 & 1 \\ 1 & 0 & 0 \\ 0 & 1 & 0 \end{bmatrix}. \tag{27}$$

Each reaction wheel inertia about its rotation axis α_i is 0.8 kg m^2. Let $C_\mathrm{srp} = 9.1e{-}6$ N/m^2, $S = 200$ m^2, and $c_\mathrm{refl} = 0.6$.

In order to implement the MPC policy (22) in a nonlinear simulation that uses (3) to propagate the satellite attitude, we must convert the attitude-error rotation matrix to Euler angles. Algorithm 1 is a method to resolve the singularities that arise from this mapping, and is adapted from [51] for the case of 3-2-1 Euler angles. Note that there exist multiple solutions for the sequence of Euler angle rotations that represent a given attitude orientation. In our simulations we select the first set of Euler angles $(\phi_1, \theta_1, \psi_1)$ if $\tilde{R}_{13}(t) \neq \pm 1$.

We consider two simulation scenarios: (i) an aggressive station-keeping and momentum unloading simulation, which highlights the MPC policy's ability to utilize the same set of thrusters, operating at their constraint limits, in order to satisfy both the force and torque requirements of station-keeping and momentum unloading, respectively, and (ii) an annual station-keeping simulation, which highlights the ability of the MPC policy to generate trajectories

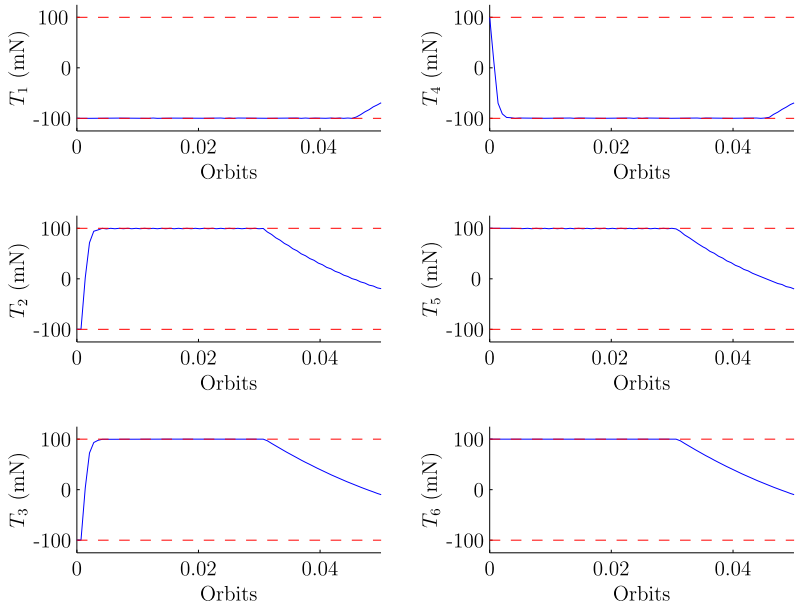

Fig. 4. Zoom of thruster time histories for aggressive station keeping and momentum unloading maneuver.

Algorithm 1 Pseudocode for calculating 3-2-1 Euler angles from the attitude-error rotation matrix.

if $\tilde{R}_{13} \neq \pm 1$ **then**
  $\theta_1 = -\arcsin(\tilde{R}_{13})$
  $\psi_1 = \text{atan2}(\frac{\tilde{R}_{12}}{\cos(\theta_1)}, \frac{\tilde{R}_{11}}{\cos(\theta_1)})$
  $\phi_1 = \text{atan2}(\frac{\tilde{R}_{23}}{\cos(\theta_1)}, \frac{\tilde{R}_{33}}{\cos(\theta_1)})$

  $\theta_2 = \pi - \theta_1$
  $\psi_2 = \text{atan2}(\frac{\tilde{R}_{12}}{\cos(\theta_2)}, \frac{\tilde{R}_{11}}{\cos(\theta_2)})$
  $\phi_2 = \text{atan2}(\frac{\tilde{R}_{23}}{\cos(\theta_2)}, \frac{\tilde{R}_{33}}{\cos(\theta_2)})$
else
  $\phi = 0$
  if $\tilde{R}_{13} = -1$ **then**
    $\theta = \frac{\pi}{2}$
    $\psi = \text{atan2}(\tilde{R}_{32}, \tilde{R}_{31})$
  else
    $\theta = -\frac{\pi}{2}$
    $\psi = \text{atan2}(-\tilde{R}_{32}, -\tilde{R}_{31})$
  end if
end if

that are comparable with carefully designed (open-loop) station-keeping techniques in terms of Δv usage.

We stress that, while the prediction model (16) is linear, the simulation is performed using the nonlinear dynamic equations (1), (3), (8). As mentioned before, we expect that the linear prediction model to be accurate because it includes the predicted contribution of the major perturbation forces, and because the MPC policy (22) enforces tight state constraints around the operating point.

We begin with the aggressive station-keeping and momentum unloading simulation. We highlight that by using the MPC policy, the satellite can perform aggressive station-keeping and momentum unloading maneuvers by using the same set of thrusters to generate both orbital forces and attitude torques. The satellite has an initial orbital displacement of $\delta x = \delta y = \delta x = 1$ km, and an initial reaction wheel spin rate $\delta \nu_i = 100$ rad/s. We discretize the dynamics with a sampling period $\Delta T = 600$ s and we set the MPC prediction horizon $N = 15$. The weighting matrices are chosen to achieve an aggressive simulation in which satellite forces and torques both operate at constraint limits and are given by

$$Q = \text{diag}(10, 10, 10, 1, 1, 1, 10^{10}, 10^{10}, 10^{17}, 10^3, 10^3, 10^3, 10^3, 10^3, 10^3),$$
$$R = 2.5 \cdot \text{diag}(10^7, 10^7, 10^7, 10^5, 10^5, 10^5, 10^6, 10^6, 10^6).$$

Fig. 3a shows that the Euler angles remain within their limits during momentum unloading, and Fig. 3b shows that the satellite relative position is brought to zero. Fig. 3e shows that the reaction wheels are aggressively decelerated, while Fig. 3c shows the time histories of the satellite forces due to the thrusters. In Figs. 3d and 3f, due to the aggressive controller tuning, we see that the forces and torques cannot concurrently operate at their individual limits. When the thrusters generate maximum torque, there is no available thrust to force the satellite towards its nominal orbital position. This effect can further be seen in Fig. 4, where individual thruster pairs such a T_1 and T_4 transition from pure torque to pure force as the reaction wheels' stored angular momentum is unloaded. Fig. 5 provides the full histories for completeness.

Next, we present the annual station-keeping simulation, where we show that MPC is capable of producing fuel-efficient station-keeping. In order to simulate an entire year, we discretize the dynamics with a sampling period $\Delta T = 3600$ s and we set the MPC prediction horizon $N = 15$. In order to minimize Δv, the weighting matrices are detuned so that the behavior of the system is driven by constraints rather than stabilizing control and are given by

$$Q = 10^{-5} \cdot \text{diag}(10^{-10}, 10, 10^{-7}, 1, 1, 1, 10^5, 10^5, 10^5, 1, 1, 1, 1, 1, 1),$$
$$R = \text{diag}(10^{15}, 10^{15}, 1, 0.1, 0.1, 0.1, 1, 1, 1).$$

Fig. 6a shows a simulation of the latitude and longitude error over one year. The satellite remains within the tight station-keeping window of ± 0.01 degrees, and in fact all the constraints of (22) are satisfied during the entire simulation at all sampling instants. Figs. 6c and 6d provide snapshots at two different times during the year of 5-day latitude and longitude trajectories in order to give a sense of the satellite motion. Fig. 6b shows the annual velocity increment Δv. In the out-of-plane z-direction, $\Delta v_z = 59$ m/s/year. In the orbital plane, $\Delta v_y = 1.6$ m/s/year and $\Delta v_x = 0.45$ m/s/year. We note that even though the station-keeping window is about one order of magnitude smaller than traditional windows,

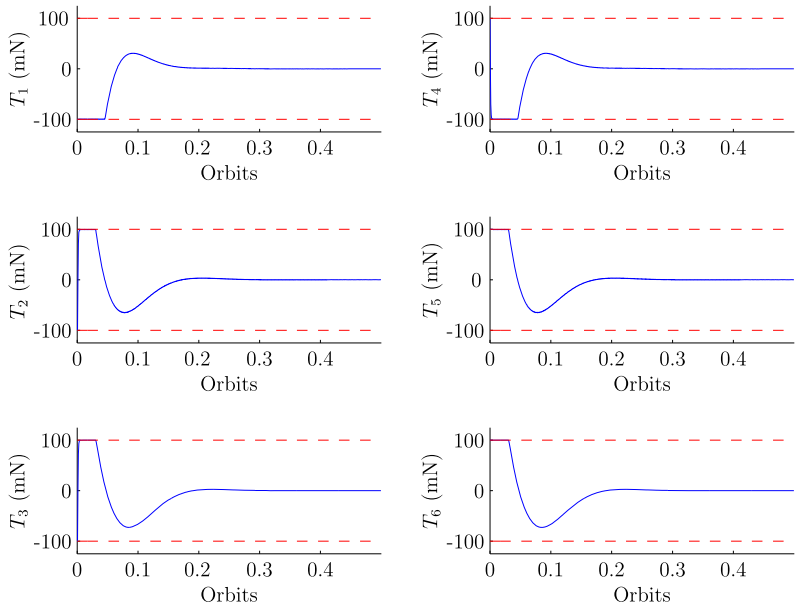

Fig. 5. Thruster time histories for aggressive station keeping and momentum unloading maneuver.

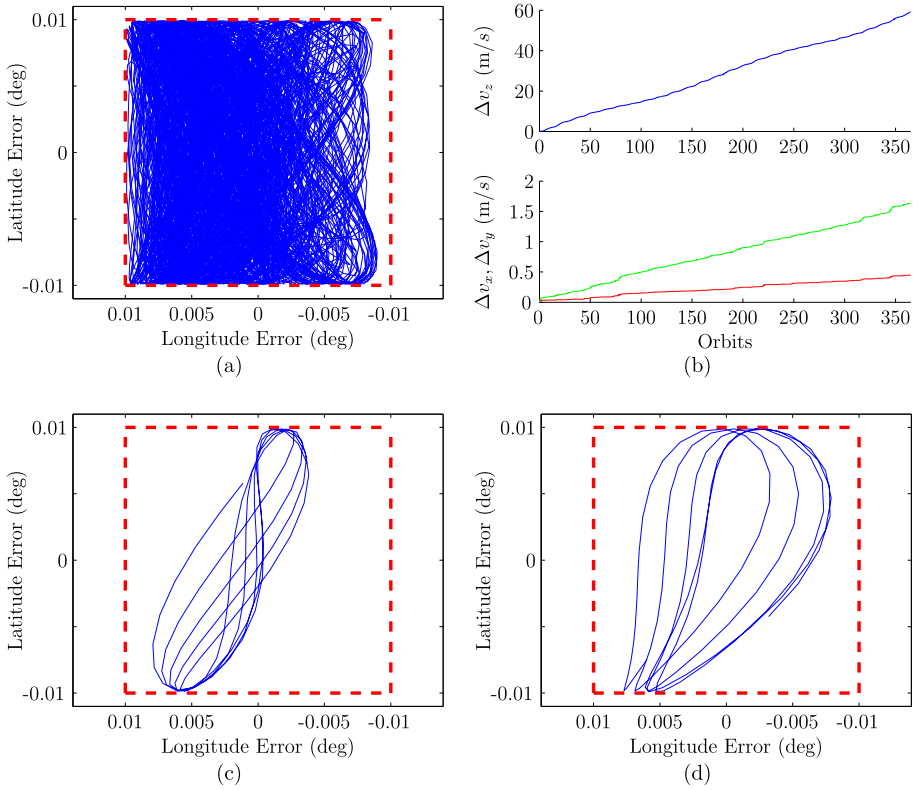

Fig. 6. Station keeping simulation: a) Annual latitude and longitude error. b) Annual velocity increment in Hill's Frame. c), d) 5-day latitude and longitude error snapshots at two different times of year.

the MPC policy is comparable in fuel usage to traditional station-keeping techniques that employ larger windows. For instance, in [11] it is claimed that for a positional accuracy of 0.05–0.1 degrees, 'North-South' Station-Keeping (NSSK), i.e., out-of-orbital-plane station-keeping, requires between 41 and 51 m/s/year, and 'East-West' Station-Keeping (EWSK) requires 1.9 m/s/year.

The design presented in this manuscript is compared to a classic LQR style controller in [37], where we show that a straightforward application of classical feedback control fails to meet the objectives laid out in Section 3. Stabilizing aggressively in order to meet station keeping requirements consumes too much fuel, while increasing the penalty on fuel violates the station keeping requirement. In this design, we are able to simultaneously achieve both objectives due to the use of station keeping constraints in conjunction with a detuned cost function. Thus, the behavior of the system is driven by a nonlinear action that thrusts only when necessary to remain in the station keeping window.

To validate the orbital dynamics model (1), including orbital perturbation effects (11), we utilize Systems Tool Kit (STK)/ Astrogator®, a high-fidelity orbit propagator developed by Ana-

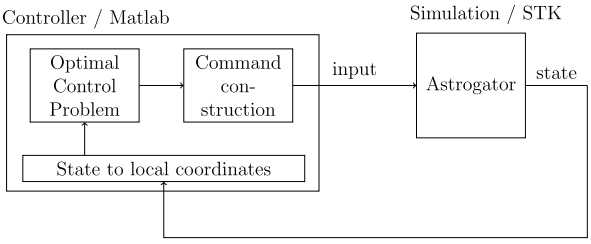

Fig. 7. Matlab and STK in closed-loop.

lytical Graphics, Inc. Fig. 8a shows an STK 3D-visualization of a geostationary satellite subject to Astrogator's flight-proven perturbations models. This open-loop simulation can be compared to that of Fig. 2b. While small discrepancies exist, the overall trends align.

Next, we close the loop between Matlab and STK. Following Fig. 7, at each control cycle we (i) feed back the satellite's true state from STK to Matlab and transform it to our local coordinates, (ii) solve the optimal control problem (22), (iii) construct the command, (iv) feed the resulting input to STK, and (v) propagate the dynamics forward in time using Astrogator. Fig. 8b shows the MPC-based station-keeping trajectory over the course of a year. Again, all the constraints of (22) are satisfied during the entire simulation at all sampling instants, and is more readily observed in Fig. 8c, which is the 2-dimensional projection of the trajectory at geostationary altitude. Fig. 8d shows the annual velocity increment Δv. In the out-of-plane z-direction, $\Delta v_z = 59.4$ m/s/year. In the orbital plane, $\Delta v_y = 1.97$ m/s/year and $\Delta v_x = 0.9$ m/s/year. Fig. 9(b)–(c) show snapshots of the satellite motion over 5 days at different times of year. The station keeping window is plotted in red; the geostationary orbit in cyan; and the satellite motion in the station keeping window in green. The results of these simulations, not only validate our detailed nonlinear model, but also the control policy's robustness and applicability for real-world implementation.

5. Conclusions

With future geostationary satellite missions requiring smaller station-keeping windows, open-loop (manual) corrections may become unsustainable. The introduction of autonomous closed-loop

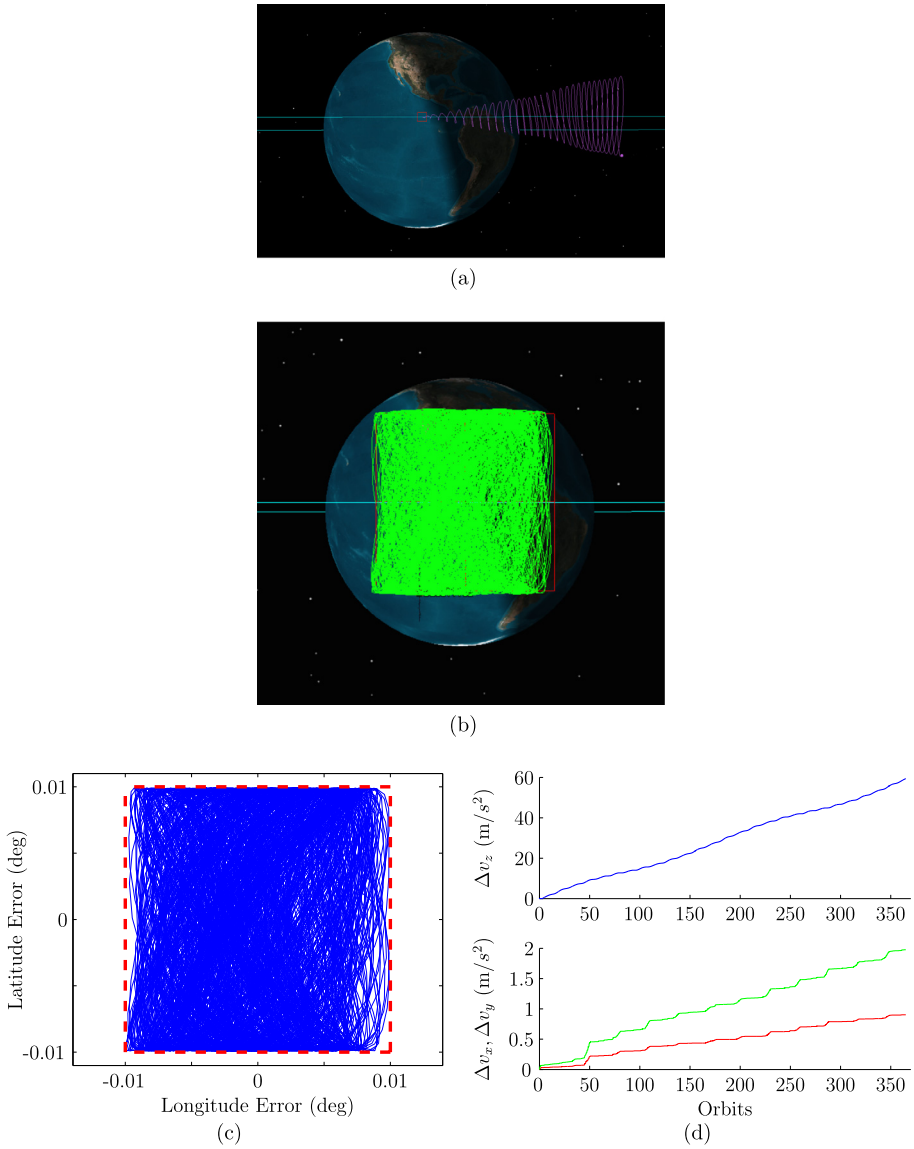

Fig. 8. STK simulations: a) One-month uncompensated geostationary satellite trajectory subject to orbital perturbations. b, c) Annual station-keeping simulation. d) Annual velocity increment in Hill's Frame.

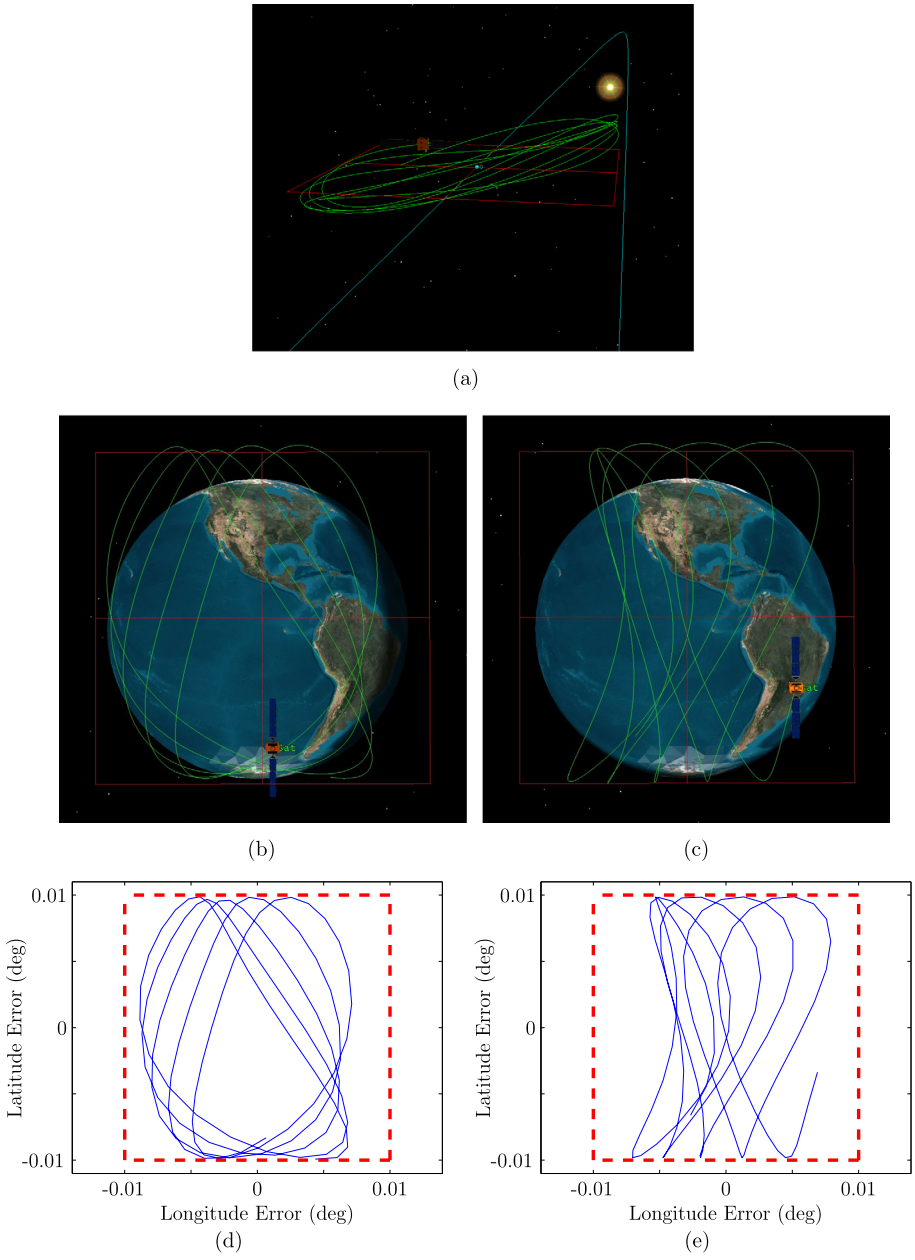

Fig. 9. STK simulations: a) 3-dimensional perspective, highlighting constraint satisfaction. b, c, d, e) 5-day satellite trajectory at two different times of year.

feedback control will increase robustness, safety and reliability of satellite station-keeping, while reducing operational costs and risk of collisions. In this paper we have developed a model predictive control (MPC) policy for autonomous closed-loop station-keeping and momentum management of a geostationary satellite. We have shown that the MPC policy satisfies the specification constraints with a fuel consumption comparable to that of carefully designed open-loop maneuvers, which, however, have significantly larger station-keeping windows. The fuel consumption performance was achieved via the use of constraints that enforce the station-keeping window, which allowed us to utilize a detuned cost function that reduces thruster usage. In addition, the proposed MPC policy is capable of concurrently performing station-keeping and momentum unloading using the same set of thrusters.

We have made some assumptions in this work that may not be entirely realistic for direct implementation in a satellite. In this work, we considered a satellite equipped with six dual-axis thrusters mounted on each face of the satellite, enabling pure thrusts and torques applied in any direction and about any axis. However, this arrangement does not leave room on the satellite's other faces for antennas and solar panels without the risk of thruster plume impingement. A more realistic design may cluster and utilize gimbaled thrusters on a single satellite face, severely restricting the control action and significantly coupling the satellite orbital and attitude dynamics. The need to treat concurrently both the "fast" attitude dynamics and the "slow" orbital dynamics may present computational challenges in resource constrained hardware. With fast dynamics, a small discretization time-step is required. However, a long MPC prediction horizon is necessary for station keeping. A small discretization time step accompanied by a long prediction horizon results in a large and computationally challenging optimization problem. Finally, in this work we assumed the ability to apply continuously variable thrust. While some advanced electric propulsion systems can throttle thrust magnitude, most systems remain on-off in nature, and yet, integer optimization methods are not practical for on-board implementa-

tion due to their complexity and cost. We plan to investigate these topics in future work.

Conflict of interest statement

No conflict.

References

[1] R.R. Bate, D.D. Mueller, J.E. White, Fundamentals of Astrodynamics, Dover Publications, 1971.
[2] P.C. Hughes, Spacecraft Attitude Dynamics, John Wiley & Sons Inc, 1986.
[3] E.M. Soop, Handbook of Geostationary Orbits, Springer, 1994.
[4] D. Losa, M. Lovera, R. Drai, T. Dargent, J. Amalric, Electric station keeping of geostationary satellites: a differential inclusion approach, in: Proc. Conf. Dec. Contr., IEEE, 2005, pp. 7484–7489.
[5] D. Chu, D. Early, D. Freesland, et al., GOES-R station-keeping and momentum management, in: Proc. of the AAS Rocky Mountain Guidance and Contr. Conf., 2006, AAS 06–046.
[6] C. Chao, J. Baker, On the propagation and control of geosynchronous orbits, J. Astronaut. Sci. 31 (1983) 99–115.
[7] S.K. Shrivastava, Orbital perturbations and stationkeeping of communication satellites, J. Spacecr. Rockets 15 (2) (1978) 67–78, https://doi.org/10.2514/3.27999.
[8] D.M. Goebel, I. Katz, Fundamentals of Electric Propulsion: Ion and Hall Thrusters, vol. 1, John Wiley & Sons, 2008.
[9] M. Sabbadini, M. Buoso, G. Saccocia, Electric Propulsion, Tech. rep., 2002.
[10] K.E. Clark, Survey of electric propulsion capability, J. Spacecr. Rockets 12 (11) (1975) 641–654, https://doi.org/10.2514/3.57030.
[11] M. Martinez-Sanchez, J.E. Pollard, Spacecraft electric propulsion—an overview, J. Propuls. Power 14 (5) (1998) 688–699, https://doi.org/10.2514/2.5331.
[12] H. Kuninaka, K. Kajiwara, Overview of JAXA's activities on electric propulsion, in: Proceedings of the 32nd International Electric Propulsion Conference, in: IEPC Paper, vol. 11, 2011, p. 332.
[13] N. Gopalswamy, J.M. Davila, F. Auchère, J. Schou, C.M. Korendyke, A. Shih, J.C. Johnston, R.J. MacDowall, M. Maksimovic, E. Sittler, et al., Earth-affecting solar causes observatory (EASCO): a mission at the sun-earth l5, in: SPIE Optical Engineering + Applications, International Society for Optics and Photonics, 2011, p. 81480Z.
[14] A. Verma, A. Fienga, J. Laskar, H. Manche, M. Gastineau, Use of messenger radioscience data to improve planetary ephemeris and to test general relativity, Astron. Astrophys. 561 (2014) A115, https://doi.org/10.1051/0004-6361/201322124.
[15] D.R. Stanbridge, K.E. Williams, A.H. Taylor, B.R. Page, C.G. Bryan, D.W. Dunham, P. Wolff, B.G. Williams, J.V. McAdams, D.P. Moessner, Achievable force model accuracies for messenger in mercury orbit, in: Astrodynamics 2011, in: Advances in the Astronautical Sciences, vol. 142, 2011.
[16] L. Beroual, D. Benatia, N. el Houda Hedjazi, High thrust station keeping maneuvers for geostationary satellites, Int. J. u- e-Serv. Sci. Technol. 8 (1) (2015) 401–414, https://doi.org/10.14257/ijunesst.2015.8.1.35.
[17] T.N. Edelbaum, Optimum low-thrust rendezvous and station keeping, AIAA J. 2 (7) (1964) 1196–1201, https://doi.org/10.2514/3.2521.
[18] A. Sukhanov, A. Prado, On one approach to the optimization of low-thrust station keeping manoeuvres, Adv. Space Res. 50 (11) (2012) 1478–1488, https://doi.org/10.1016/j.asr.2012.07.028.
[19] V.M. Gomes, A.F. Prado, Low-thrust out-of-plane orbital station-keeping maneuvers for satellites, Math. Probl. Eng. (2012), https://doi.org/10.1155/2012/532708.
[20] F. Topputo, F. Bernelli-Zazzera, Optimal low-thrust stationkeeping of geostationary satellites, in: Proceedings of Confederation of European Aerospace Societies Conference, Confine Edizioni Monghidoro, Bologna, 2011, pp. 1917–1925.
[21] D. Losa, High vs Low Thrust Station Keeping Maneuver Planning for Geostationary Satellites, Ph.D. thesis, École Nationale Supérieure des Mines de Paris, 2007.
[22] J.R. Wertz, W.J. Larson, Space Mission Analysis and Design, Microcosm, 1999.
[23] J.B. Rawlings, D.Q. Mayne, Model Predictive Control: Theory and Design, Nob Hill, Madison, Wisconsin, 2009.
[24] J.A. Starek, I. Kolmanovsky, Nonlinear model predictive control strategy for low thrust spacecraft missions, Optim. Control Appl. Methods 35 (1) (2014) 1–20, https://doi.org/10.1002/oca.2049.
[25] M. Leomanni, A. Garulli, A. Giannitrapani, F. Scortecci, All-electric spacecraft precision pointing using model predictive control, J. Guid. Control Dyn. 38 (1) (2014) 161–168, https://doi.org/10.2514/1.G000347.
[26] S. Boyd, L. Vandenberghe, Convex Optimization, Cambridge University Press, 2004.
[27] D.P. Bertsekas, Dynamic Programming and Optimal Control, vol. 2, Athena Scientific, Belmont, MA, 2012.
[28] S. Richter, C.N. Jones, M. Morari, Computational complexity certification for real-time MPC with input constraints based on the fast gradient method, IEEE Trans. Autom. Control 57 (6) (2012) 1391–1403, https://doi.org/10.1109/tac.2011.2176389.
[29] P. Patrinos, A. Bemporad, An accelerated dual gradient-projection algorithm for embedded linear model predictive control, IEEE Trans. Autom. Control 59 (1) (2014) 18–33, https://doi.org/10.1109/tac.2013.2275667.
[30] M. Kögel, R. Findeisen, A fast gradient method for embedded linear predictive control, in: Proc. IFAC World Congress, Milan, Italy, 2011, pp. 1362–1367.
[31] S. Di Cairano, M. Brand, S.A. Bortoff, Projection-free parallel quadratic programming for linear model predictive control, Int. J. Control 86 (8) (2013) 1367–1385, https://doi.org/10.1080/00207179.2013.801080.
[32] P. Giselsson, S. Boyd, Linear convergence and metric selection in Douglas–Rachford splitting and ADMM, IEEE Trans. Autom. Control (99) (2016) 1, https://doi.org/10.1109/tac.2016.2564160.
[33] E. Ghadimi, A. Teixeira, I. Shames, M. Johansson, Optimal parameter selection for the alternating direction method of multipliers (ADMM): quadratic problems, IEEE Trans. Autom. Control 60 (3) (2015) 644–658, https://doi.org/10.1109/tac.2014.2354892.
[34] A.U. Raghunathan, S. Di Cairano, Alternating direction method of multipliers for strictly convex quadratic programs: optimal parameter selection, in: American Control Conf., 2014, pp. 4324–4329.
[35] A.U. Raghunathan, S. Di Cairano, ADMM for convex quadratic programs: linear convergence and infeasibility detection, arXiv preprint, arXiv:1411.7288.
[36] A. Weiss, U. Kalabić, S. Di Cairano, Model predictive control for simultaneous station keeping and momentum management of low-thrust satellites, in: American Control Conference, ACC 2015, IEEE, 2015, pp. 2305–2310.
[37] A. Weiss, S. Di Cairano, Opportunities and potential of model predictive control for low-thrust spacecraft station-keeping and momentum-management, in: 2015 European Control Conference (ECC), IEEE, 2015, pp. 1370–1375.
[38] U. Kalabić, A. Weiss, I. Kolmanovsky, S. Di Cairano, Station-keeping and momentum-management on halo orbits around L2: linear-quadratic feedback and model predictive control approaches, in: Proceedings of 25th AAS/AIAA Space Flight Mechanics Meeting, 2015, AAS-15-307.
[39] W. Clohessy, R. Wiltshire, Terminal guidance system for satellite rendezvous, J. Aerosp. Sci. 27 (9) (1960) 653–658, https://doi.org/10.2514/8.8704.
[40] B. Wie, Space Vehicle Dynamics and Control, 2nd edition, AIAA, Reston, VA, 2008.
[41] A. Weiss, I. Kolmanovsky, D.S. Bernstein, A. Sanyal, Inertia-free spacecraft attitude control using reaction wheels, J. Guid. Control Dyn. 36 (5) (2013) 1425–1439, https://doi.org/10.2514/1.58363.
[42] A.H. de Ruiter, C. Damaren, J.R. Forbes, Spacecraft Dynamics and Control: An Introduction, John Wiley & Sons, 2012.
[43] S. Keerthi, E.G. Gilbert, Optimal infinite-horizon feedback laws for a general class of constrained discrete-time systems: stability and moving-horizon approximations, J. Optim. Theory Appl. 57 (2) (1988) 265–293, https://doi.org/10.1007/bf00938540.
[44] E. Gilbert, K. Tan, Linear systems with state and control constraints: the theory and applications of maximal output admissible sets, IEEE Trans. Autom. Control 36 (9) (1991) 1008–1020, https://doi.org/10.1109/9.83532.
[45] S. Di Cairano, A. Bemporad, Model predictive control tuning by controller matching, IEEE Trans. Autom. Control 55 (1) (2010) 185–190, https://doi.org/10.1109/tac.2009.2033838.
[46] D. Limon, T. Alamo, D. Raimondo, D.M. de la Pena, J. Bravo, A. Ferramosca, E. Camacho, Input-to-state stability: a unifying framework for robust model predictive control, in: Nonlinear Model Predictive Control, Springer, 2009, pp. 1–26.
[47] Model predictive idle speed control: design, analysis, and experimental evaluation, IEEE Trans. Control Syst. Technol. 20 (1) (2012) 84–97, https://doi.org/10.1109/tcst.2011.2112361.
[48] R. Fletcher, Practical Methods of Optimization, John Wiley & Sons, 2013.
[49] Y. Nesterov, Introductory Lectures on Convex Optimization, vol. 87, Springer Science & Business Media, 2004.
[50] H. Ferreau, S. Almér, R. Verschueren, M. Diehl, D. Frick, A. Domahidi, J. Jerez, G. Stathopoulos, C. Jones, Embedded optimization methods for industrial automatic control, in: Proceedings of the IFAC World Congress, 2017.
[51] G. Slabaugh, Computing Euler Angles from a Rotation Matrix, Tech. rep., City Univ. London, London, UK, 1999.